Appl Phys B (2009) 96: 749–755
DOI 10.1007/s00340-009-3527-7

Applied Physics B
Lasers and Optics

Transition between corrugated metal films and split-ring-resonator arrays

C.E. Kriegler · M.S. Rill · M. Thiel · E. Müller · S. Essig · A. Frölich · G. von Freymann · S. Linden · D. Gerthsen · H. Hahn · K. Busch · M. Wegener

Received: 2 February 2009 / Revised version: 19 March 2009 / Published online: 5 May 2009

Abstract We fabricate split-ring-resonator arrays via direct laser writing of polymers, followed by atomic-layer deposition of titania, chemical vapor deposition of silver, and focused-ion-beam milling. While structures like that have been fabricated previously by other means, our approach here allows for a direct comparison with the optical properties of corrugated metal surfaces, which are fabricated along the same lines. This comparison reveals substantial differences regarding the magnetic metamaterial properties. In particular, we find that the optical response of the corrugated metal surfaces is due to a higher-order magnetic resonance, whereas that of the split-ring resonators stems from their fundamental magnetic resonance.

C.E. Kriegler · M.S. Rill (✉) · M. Thiel · A. Frölich · G. von Freymann · S. Linden · M. Wegener
Institut für Angewandte Physik, Universität Karlsruhe (TH), Wolfgang-Gaede-Straße 1, 76131 Karlsruhe, Germany
e-mail: michael.rill@physik.uni-karlsruhe.de
Fax: +49-721-6088480

C.E. Kriegler · M.S. Rill · M. Thiel · E. Müller · S. Essig · A. Frölich · G. von Freymann · S. Linden · D. Gerthsen · H. Hahn · K. Busch · M. Wegener
DFG-Center for Functional Nanostructures (CFN), Universität Karlsruhe (TH), 76128 Karlsruhe, Germany

G. von Freymann · S. Linden · H. Hahn · M. Wegener
Institut für Nanotechnologie, Forschungszentrum Karlsruhe in der Helmholtz-Gemeinschaft, 76021 Karlsruhe, Germany

E. Müller · D. Gerthsen
Laboratorium für Elektronenmikroskopie, Universität Karlsruhe (TH), 76128 Karlsruhe, Germany

S. Essig · K. Busch
Institut für Theoretische Festkörperphysik, Universität Karlsruhe (TH), 76128 Karlsruhe, Germany

PACS 42.70.-a · 81.16.Nd · 81.15.Gh

1 Introduction

Split-ring resonators [1, 2] are crucial functional building blocks of man-made photonic metamaterials (see also the recent reviews [3–5]). Using these "photonic atoms" allows for achieving strong effective (dia-) magnetism at optical frequencies—which is inaccessible for all known natural substances. In essence, split-ring resonators (SRR) can be viewed as tiny metallic sub-wavelength resonant electromagnets. They are composed of an almost closed metallic loop forming an inductor with inductance L. The ends of the metallic wire form a capacitor with capacitance C, as illustrated in Fig. 1. In a more refined modeling, the surface capacitance should also be taken into account [6]. For frequencies ω above the SRR LC eigenfrequency, $\omega_{LC} = (LC)^{-1/2}$, in close analogy to any har-

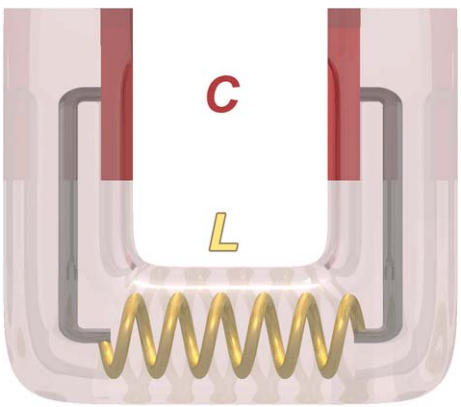

Fig. 1 A split-ring resonator can be considered as an LC circuit

monic oscillator, the response is phase delayed by 180 degrees with respect to the driving force. Hence, the local magnetic field of the SRR is opposite to the external magnetic field, resulting in a diamagnetic behavior. For sufficiently strong diamagnetism, the effective magnetic permeability μ of the resulting effective material can become negative [2–5].

Recently, a variation of this general scheme has been discussed in the form of corrugated metal films (see Fig. 2a) [7–9]. At first sight, this geometry appears to be only a minor modification of a two-dimensional array of isolated SRR (Fig. 2d)—that have been fabricated previously [10]—in that the SRR are "simply" electrically connected along the two in-plane directions (also compare Figs. 2b and c). Yet, as we will show in this paper by fabrication and direct comparison of the optical properties for what we believe is the first time, a closer inspection reveals fundamental differences between these cases. This is evidenced by characterization of the resulting structures via optical transmittance spectroscopy, the results of which are compared with numerical calculations. Representative snapshots of the calculated ohmic current density distributions further highlight the differences between corrugated metal films and electrically isolated SRR. Finally, we give an intuitive interpretation of our findings.

2 Results and discussion

2.1 Fabrication

Fabrication starts with a glass substrate covered with a 2-µm-thick fully polymerized resist film (SU-8). If this layer is not present, the different thermal expansion coefficients of the glass substrate and the SU-8 structure cause tearing of the coated silver layer during the metallization process at higher temperatures. Subsequently, another SU-8 film is spun-on and exposed using direct laser writing (DLW) [11], post-baked and developed. DLW is a well established technique for fabricating three-dimensional polymeric micro- and nanostructures by tightly focusing femtosecond laser pulses into the volume of a photoresist and scanning the sample in three dimensions. For the case of the negative-tone commercial photoresist SU-8 (MicroChem Corp.), only those parts which have been sufficiently exposed by two-photon absorption of light remain after the development process. Here, we employ a commercial DLW system (Nanoscribe GmbH; see www.nanoscribe.de) that especially allows for automated finding of the glass-polymer interface—an aspect which is crucial for our structures. Furthermore, the system allows for automated tilt-correction between the substrate surface and the scanning plane. Without this feature, one typically obtains substantial lateral gradients in height within the sample footprint (here 50 µm × 50 µm).

Next, the resulting polymer template is mechanically and chemically protected by a thin dielectric layer. Unlike in our previous work [9], we do not use silica (SiO_2) here but rather employ amorphous titania (TiO_2), deposited via atomic-layer deposition (ALD) at 110°C using titanium tetrachloride ($TiCl_4$) and H_2O as precursors [12, 13]. From our experience, the resulting surfaces are advantageous compared to SiO_2 for growth of smooth thin silver films (see below). Furthermore, the commercial apparatus used for the TiO_2 ALD (Savannah S-100 by Cambridge NanoTech, Inc.) leads to more controlled and more reproducible layer thicknesses than our previous home-built SiO_2 ALD [9, 14, 15].

For the silver chemical-vapor deposition (CVD), the template is heated to 165°C. The metal-organic precursor (1, 5-COD)(hfac)Ag(I) (99%, Sigma-Aldrich, Inc.) is sublimed at a temperature of 70°C, and the wall temperature of the CVD chamber is 80°C. In each static cycle of 40 minutes in duration, we deposit about 2 nm of silver. The samples to be discussed below have resulted from 15 CVD cycles, equivalent to an estimated silver thickness of about 34 nm. Note that this film is thinner than the one previously reported [9]. Notably, the film is still closed and smooth on the standards of silver CVD [16].

For the structure shown as electron micrograph in Fig. 3a, the processing stops at this point. The other structures shown in Fig. 3 have been post-processed by focused-ion-beam (FIB) milling (see, e.g., Ref. [17]). We use a FIB/SEM (scanning electron microscopy) system (Zeiss 1540 XB) operating with Ga^+ ions at 30 keV. Milling along the grooves is performed manually by imaging the trenches with an ion beam of 20 pA. For orthogonal cuts in Figs. 3c and d an ELPHY Plus Raith nanolithography system is utilized for automatically controlling the FIB milling with a beam current of 100 pA.

Clearly, the electron micrographs of the fabricated structures in Fig. 3 come fairly close to the desired ideal, which has been schematically depicted in Figs. 2a–d.

2.2 Spectroscopic results

To determine the optical properties of the metamaterial layers, we have measured normal-incidence transmittance spectra using a Fourier-transform spectrometer (Bruker Equinox 55, near-infrared halogen source) in combination with a microscope (Bruker Hyperion 2000, ×36 Cassegrain objectives, numerical aperture: 0.5, liquid-N_2-cooled InSb detector). All results shown in Fig. 4 are for linear polarization of the incident light, oriented perpendicular to the grooves of the original corrugated metal film (see Figs. 2e and 3a). All spectra are normalized to the transmittance

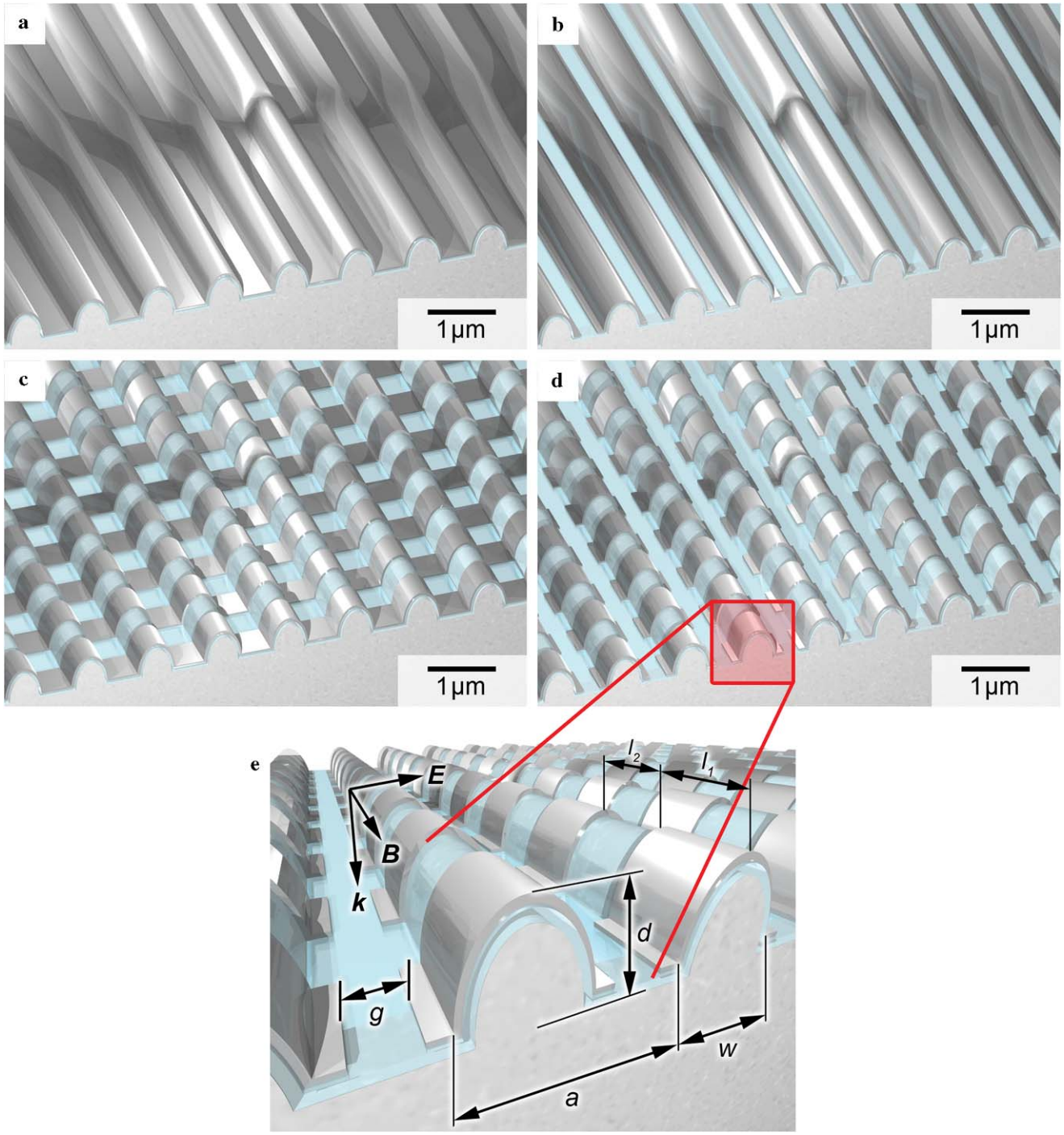

Fig. 2 Illustration of the four different cases of magnetic metamaterial layers discussed in this work. **a** Corrugated metal film; **b** one-dimensional array of electrically separated elongated split-ring resonators; **c** one-dimensional array of laterally connected split-ring resonators; **d** two-dimensional array of electrically separated split-ring resonators. **e** Incident polarization and definition of geometrical parameters. In **a**–**e**, the polymer, the titania, and the silver layer are shown by light gray, blue, and glossy gray, respectively

of the bare glass substrate. The transmittance for sample (a) reproduces the overall behavior already discussed in our previous work [9] on corrugated metal films. The transmittance minimum highlighted by the gray shading corresponds to the excitation of a magnetic-dipole resonance. FIB milling along the grooves leads to sample (b), which reveals a transmittance minimum that is substantially shifted towards longer wavelengths. Milling along the vertical direction in (c) and (d) only leads to a minor additional shift towards longer wavelengths. The latter aspect is well under-

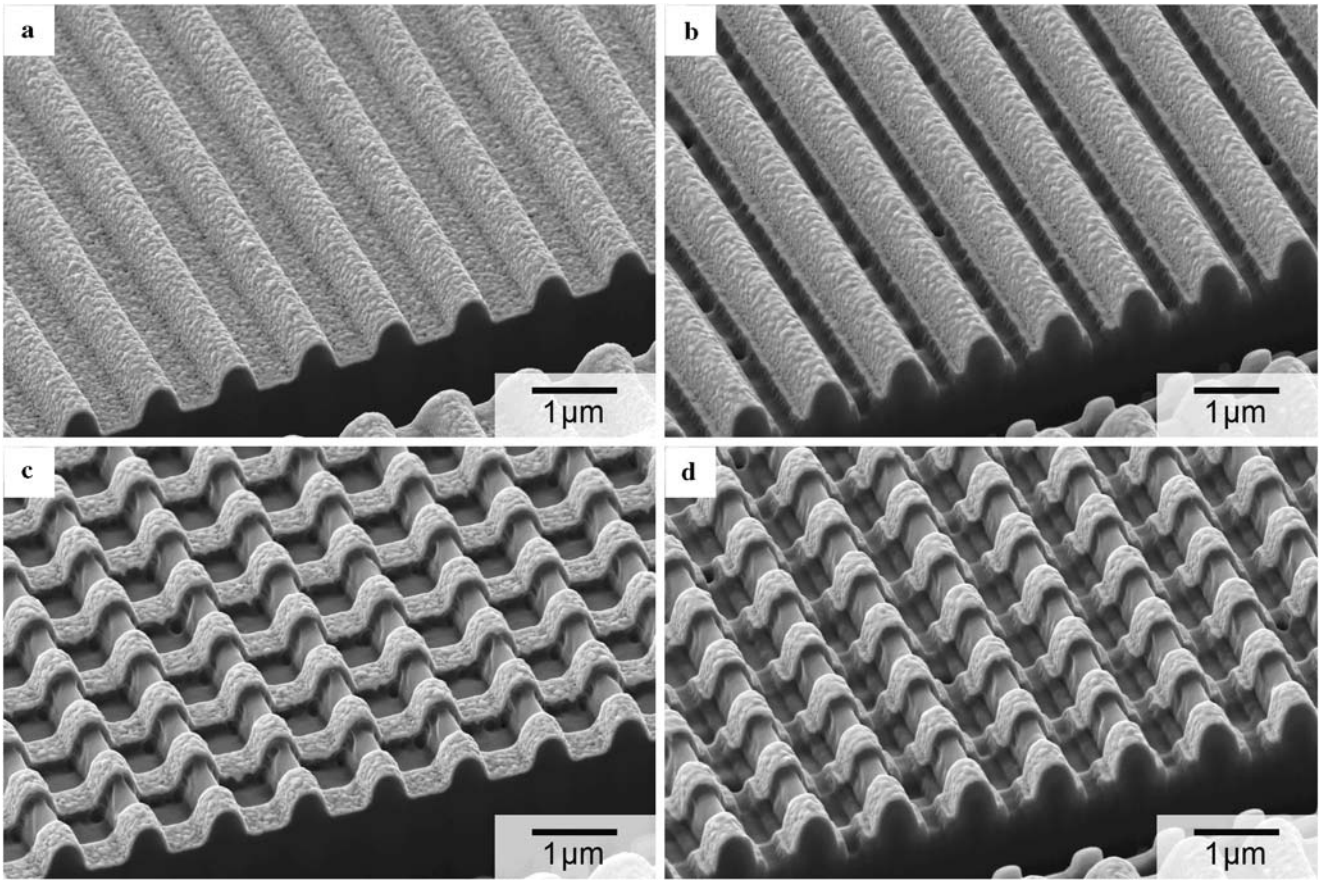

Fig. 3 Oblique-view electron micrographs of representative regions of the fabricated metamaterial structures. The four cases correspond to those shown in Fig. 2. **a** is realized by direct laser writing and subsequent silver metallization via CVD, cases **b–d** have required additional post-processing by means of FIB milling

stood and stems from the fact that flat SRR have a lower fundamental resonance frequency than elongated SRR [2, 18].

To allow for direct comparison with the theoretical ideal, we solve the vector Maxwell equations numerically for one 3D unit cell with waveguide boundary conditions using the finite integration technique (FIT) software package CST Microwave Studio. Furthermore, we check the results for the purely two-dimensional structures, i.e., cases (a) and (b), with a home-made Fourier modal method code (scattering-matrix approach) [19, 20] by employing an expansion of the fields in 801 plane waves. The 2D unit cell is subdivided into 524 layers along the propagation direction of the incident light wave (see Fig. 2e) and calculated by using periodic boundary conditions. The complex geometrical parameters are illustrated in Fig. 2: periodicity $a = 1000$ nm, width $w = 570$ nm, height $d = 525$ nm, length $l_1 = 550$ nm, length $l_2 = 450$ nm, width of FIB-milled grooves $g = 270$ nm. As usual, the silver optical properties are described by the free-electron Drude model with plasma frequency $\omega_{\mathrm{pl}} = 1.37 \times 10^{16}\ \mathrm{s}^{-1}$ and collision frequency $\omega_{\mathrm{col}} = 8.50 \times 10^{13}\ \mathrm{s}^{-1}$ [21]. The refractive indices of SU-8 and titania (TiO_2) [22] are taken as $n_{\mathrm{SU\text{-}8}} = 1.57$ and $n_{\mathrm{titania}} = 2.05$, respectively. Calculated transmittance spectra are shown in Fig. 5. Obviously, all experimental findings of Fig. 4 are very well reproduced. Especially, the resonance positions (compare gray regions) agree qualitatively. Remaining quantitative discrepancies are likely due to simplifications in the considered model geometry and/or due to fabrication imperfections. In particular, it is known that FIB milling tends to introduce Ga contamination, deteriorating the optical properties.

To clarify the nature of the resonances and to clarify the observed difference between the two cases (a) and (b), we depict characteristic snapshots of the computed current inside the metal film in Figs. 6a and b. The size of the arrows shown in these cross sections is linearly proportional to the absolute value of the local ohmic current density vector (at this point in time). For case (a), the currents correspond to the SRR (see also Fig. 1) schematically shown in light red in the background ("U"). In contrast, for case (b), the currents rather correspond to SRR that are shifted laterally and turned upside down with respect to the substrate plane.

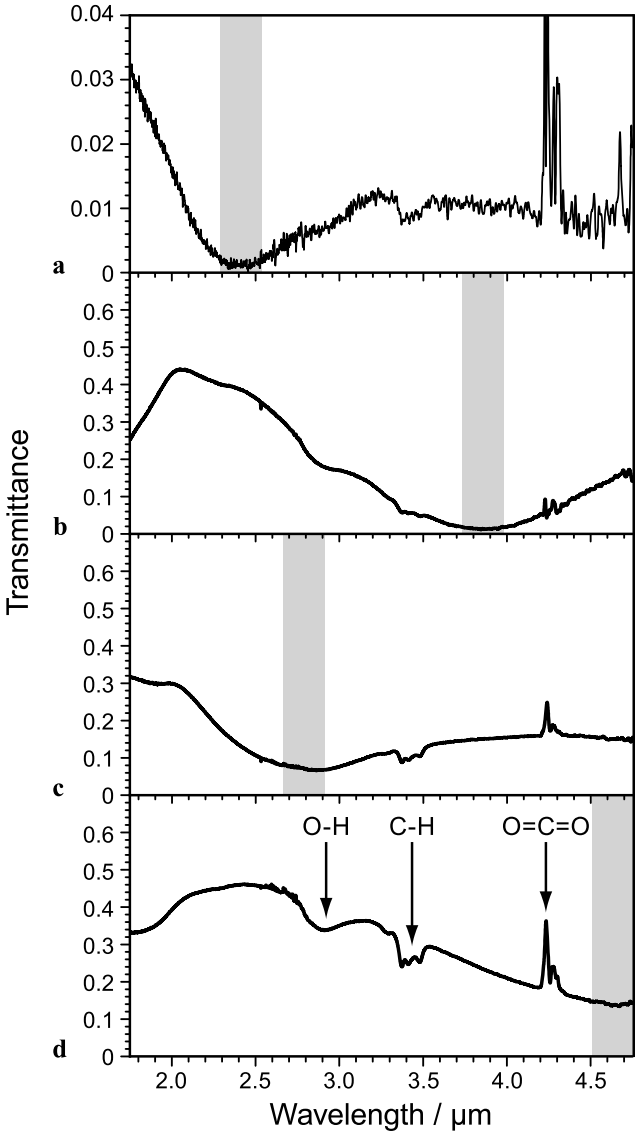

Fig. 4 Measured normal-incidence (intensity) transmittance spectra for the four samples shown in Fig. 3. To guide the eye, the gray regions highlight the magnetic resonance in each case. For clarity, the vertical scales are chosen differently. Artifacts resulting from absorption lines are indicated in **d**

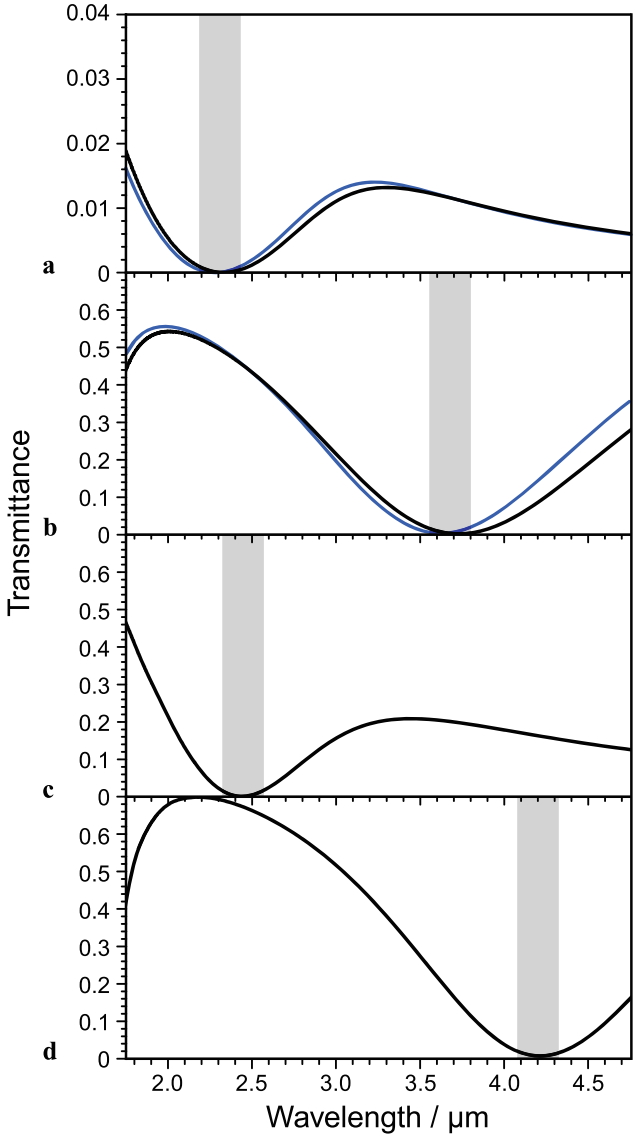

Fig. 5 Calculated spectra corresponding to the measured ones depicted in Fig. 4. In **a** and **b** finite integration technique calculations (*black*) are compared with Fourier modal method calculations (*blue*) using the same geometrical parameters. Note that the scales of Figs. 4 and 5 are identical, allowing for a direct comparison. The geometry considered is shown in Fig. 2

2.3 Discussion

Let us discuss this key aspect in an intuitive manner. For the case (b) of separated SRR, the fundamental *LC* resonance is clearly that of an upside down "U" (see Fig. 6b). The oscillating circulating currents and, hence, the magnetic dipoles are induced by the voltage drop over the two ends of the plate capacitor part of the SRR (compare Fig. 1) and, simultaneously, by the time-dependent magnetic field normal to the plane depicted in Fig. 6. It is this combination which gives rise to bi-anisotropy [9, 23–25]. The case (a) of a corrugated metal film is more sophisticated. Here, the right-hand side plate of one SRR is electrically connected to the left-hand side plate of the SRR to its right. As the metamaterial structure is excited via a plane electromagnetic wave under normal incidence, all fictitious SRR are forced to oscillate in phase. In other words: All SRR are forced to have the same potential difference between their left and right-hand side plate. Combined with the discussed electric connection of neighboring SRR, this is essentially equivalent to short-circuiting each plate capacitor, i.e., each split-ring becomes a closed ring. Successively closing the gap of a "U" towards an "O" corresponds to a diverging capacitance *C* (inversely proportional to the plate separation) and, thus, to a fundamental *LC* eigenfrequency of the SRR approaching zero

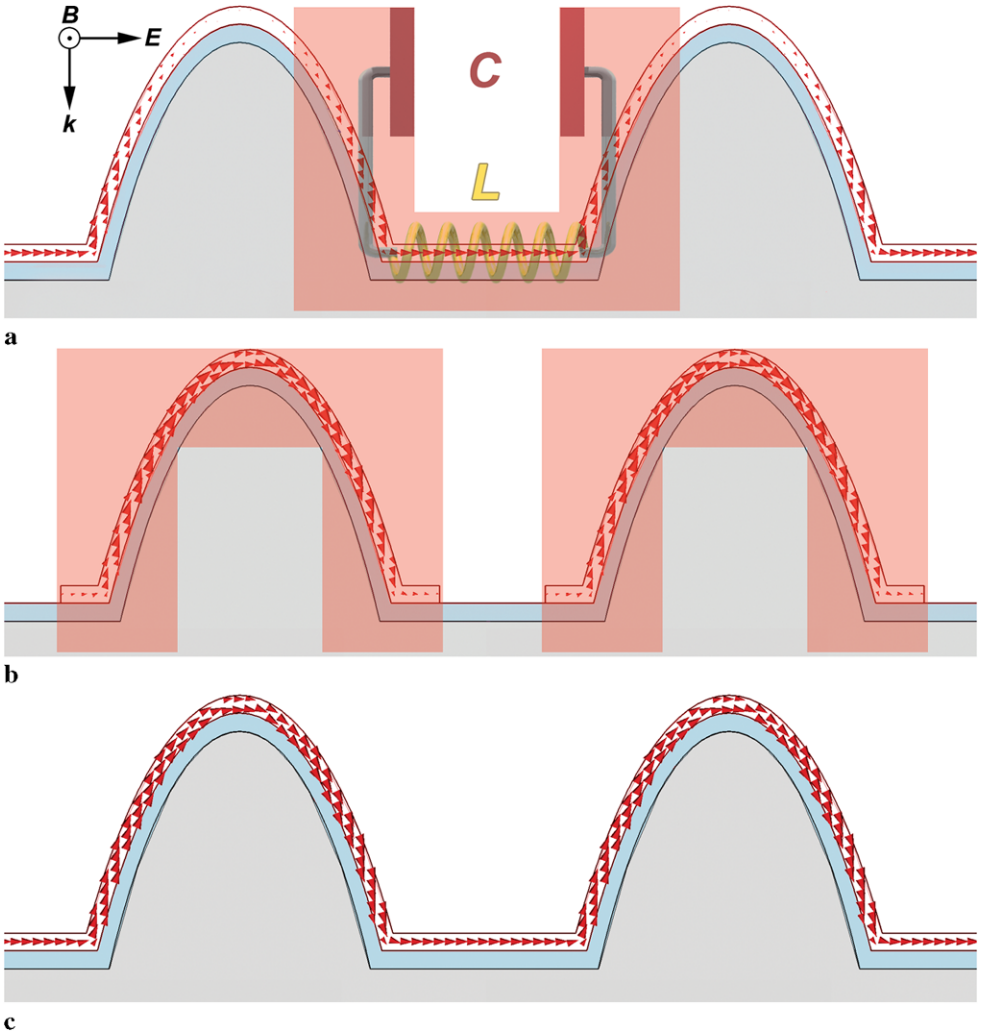

Fig. 6 Snapshots of the ohmic current density inside the metal layer calculated by using the finite integration technique. For clarity, a second unit cell is added to the actually calculated volume. Case **a** corresponds to the resonance wavelength of 2.38 µm shown in Fig. 5a, **b** to the resonance wavelength of 3.75 µm shown in Fig. 5b. Case **c** is for the identical structure as in **a**, but for 300 µm wavelength (corresponding frequency of 1 THz) of light (i.e., essentially the static limit). The red areas in **a** and **b** illustrate our intuitive interpretation (also compare Fig. 1)

[2, 5]. Indeed, in the quasi-static case (at 1 THz $\ll$ 126 THz) additionally shown in Fig. 6c, strong circulating oscillating currents leading to strong magnetic dipoles excited by the incident light field survive—in sharp contrast to what is known for separated SRR. This situation is roughly similar to applying the two poles of a battery at the left and right-hand side end of the structure shown in Fig. 2a. Clearly, the voltage drop between the two ends leads to an electric current flowing from the left to the right that will create local magnetic dipoles in the almost closed metallic loops. If (and only if) the structure is asymmetric, precisely if it lacks inversion symmetry along the propagation direction, the neighboring magnetic-dipole moments do not cancel and a net magnetization of the metamaterial structure survives even in the static limit. For electrically separated SRR like the ones shown in Fig. 2b, this continuous current flow is obviously not possible.

Thus, the transmittance resonance observed in the experiment in Fig. 4a for the corrugated metal film is not the fundamental magnetic resonance but rather a higher-order mode. The fundamental mode of the system shifts towards zero frequency (infinite wavelength) when going from case (b) to case (a)—in contrast to what one might have concluded from the spectra shown in Fig. 4 at first sight.

3 Conclusions

In summary, using focused-ion beam post-processing of structures made via direct laser writing and subsequent metallization by means of chemical-vapor deposition, we have realized a set of metamaterial structures illustrating the systematic transition from a corrugated metal film to one- and two-dimensional arrays of separated SRR that are electrically isolated from one another. We find that the corrugated metal film has its "fundamental resonance" at zero frequency. Hence, the finite-frequency magnetic resonance observed here, and also reported in previous studies, should rather be viewed as a higher-order magnetic resonance.

Acknowledgements We thank Ekmel Ozbay and Costas M. Soukoulis for discussions. We acknowledge the support of the Deutsche Forschungsgemeinschaft (DFG) and the State of Baden-Württemberg

through the DFG-Center for Functional Nanostructures (CFN) within subprojects A1.1, A1.4, and A1.5. The project PHOME acknowledges the financial support of the Future and Emerging Technologies (FET) programme within the Seventh Framework Programme for Research of the European Commission, under FET-Open grant number 213390. Also, we acknowledge funding through the METAMAT project by the Bundesministerium für Bildung und Forschung (BMBF). The research of S.L. is also supported through a Helmholtz-Hochschul-Nachwuchsgruppe (VH-NG-232), the research of G.v.F. through the DFG Emmy-Noether fellowship (FR 1671/4-3). The PhD education of C.E.K., M.S.R., M.T. and S.E. is further supported by the Karlsruhe School of Optics and Photonics (KSOP). The Fourier modal method computations have been performed on HP XC4000 at Steinbuch Center for Computing (SCC) Karlsruhe under project NOTAMAX.

References

1. W.N. Hardy, L.A. Whitehead, Rev. Sci. Instrum. **52**, 213 (1981)
2. J.B. Pendry, A.J. Holden, D.J. Robbins, W.J. Stewart, IEEE Trans. Microwave Theory Tech. **47**, 2075 (1999)
3. V.M. Shalaev, Nat. Photonics **1**, 41 (2007)
4. C.M. Soukoulis, S. Linden, M. Wegener, Science **315**, 47 (2007)
5. K. Busch, G. von Freymann, S. Linden, S.F. Mingaleev, L. Tkeshelashvili, M. Wegener, Phys. Rep. **444**, 101 (2007)
6. O. Sydoruk, E. Tatartschuk, E. Shamonina, L. Solymar, J. Appl. Phys. **105**, 014903 (2009)
7. U. Schröter, D. Heitmann, Phys. Rev. B **60**, 4992 (1999)
8. H. Schweizer, L. Fu, H. Gräbeldinger, H. Guo, N. Liu, S. Kaiser, H. Giessen, Phys. Status Solidi A **204**, 3886 (2007)
9. M.S. Rill, C. Plet, M. Thiel, I. Staude, G. von Freymann, S. Linden, M. Wegener, Nat. Mater. **7**, 543 (2008)
10. S. Zhang, W. Fan, B.K. Minhas, A. Frauenglass, K.J. Malloy, S.R.J. Brueck, Phys. Rev. Lett. **94**, 037402 (2005)
11. S. Kawata, H.-B. Sun, T. Tanaka, K. Takada, Nature **412**, 697 (2001)
12. M. Ritala, M. Leskelä, E. Nykänen, P. Soininen, L. Niinistö, Thin Solid Films **225**, 288 (1993)
13. J. Aarik, A. Aidla, A.-A. Kiisler, T. Uustare, V. Sammelselg, Thin Solid Films **305**, 270 (1997)
14. D.J. Ehrlich, J. Melngailis, Appl. Phys. Lett. **58**, 2675 (1991)
15. M. Hermatschweiler, A. Ledermann, G.A. Ozin, M. Wegener, G. von Freymann, Adv. Funct. Mater. **17**, 2273 (2007)
16. A. Grodzicki, I. Łakomska, P. Piszczek, I. Szymańska, E. Szłyk, Coord. Chem. Rev. **249**, 2232 (2005)
17. C. Enkrich, F. Pérez-Willard, D. Gerthsen, J. Zhou, T. Koschny, C.M. Soukoulis, M. Wegener, S. Linden, Adv. Mater. **17**, 2547 (2005)
18. H. Guo, N. Liu, L. Fu, H. Schweizer, S. Kaier, H. Giessen, Phys. Status Solidi B **244**, 1256 (2007)
19. L. Li, J. Opt. Soc. Am. A **14**, 2758 (1997)
20. P. Lalanne, M.P. Jurek, J. Mod. Opt. **45**, 1357 (1998)
21. G. Dolling, M. Wegener, S. Linden, Opt. Lett. **32**, 551 (2007)
22. J. Rodrígues, M. Gómez, J. Ederth, G.A. Niklasson, C.G. Grandvist, Thin Solid Films **365**, 119 (2000)
23. R. Marqués, F. Medina, R. Rafii-El-Idrissi, Phys. Rev. B **65**, 144440 (2002)
24. D.R. Smith, S. Schultz, P. Markoš, C.M. Soukoulis, Phys. Rev. B **65**, 195104 (2002)
25. X. Chen, B.-I. Wu, J.A. Kong, T.M. Grzegorczyk, Phys. Rev. E **71**, 046610 (2005)